photonics

MDPI

Article

Influence of Exposure Parameters on Nanoliquid-Assisted Glass Drilling Process Using CO_2 Laser

Mohaimen Najah Mahdi [1], Ahmed Issa [2], Hala Salman Hasan [1], Ahmed R. Al-Hamaoy [3] and Muammel M. Hanon [4,*]

[1] Department of Mechanical Engineering, College of Engineering, Al-Nahrain University, Jadriya, Baghdad 64040, Iraq
[2] Mechatronics and Medical Devices Engineering Department, Faculty of Engineering and Information Technology, Al-Azhar University – Gaza, Gaza 1277, Palestine
[3] Department of Laser & Optoelectronics Engineering, College of Engineering, Al-Nahrain University, Jadriya, Baghdad 64040, Iraq
[4] Baquba Technical Institute, Middle Technical University, Baghdad 10074, Iraq
* Correspondence: muammel.m.hanon@mtu.edu.iq

Abstract: Liquid-assisted laser processing (LALP) is implemented using a 10.6 µm continuous-wave (CW) CO_2 laser to drill holes in 1.1 mm thick soda-lime glass substrates fully immersed in a nanoliquid bath. The nanoliquid bath consisted of de-ionized water and carbon nano-particles (CNPs) of different wt.%. The study focuses on the influence of exposure time (T_E, [s]), laser beam power (P, [W]) and number of pulses (N_P) on resulting geometrical features, namely, crack length (CL, [mm]), inlet diameter (D_{INLET}, [mm]) and exit diameter (D_{EXIT}, [mm]). The processed samples were characterized using an optical microscope. Findings show that LALP with investigated ranges of control parameters T_E (0.5–1.5 s), P (20–40 W) and N_P (1–6 pulses) led to successful production of drilled holes having CL range (0.141 to 0.428 mm), D_{INLET} range (0.406 to 1.452 mm) and D_{EXIT} range (0.247 to 1.039 mm). It was concluded that increasing T_E alone leads to increasing CL, D_{INLET} and D_{EXIT}, while keeping a good balance among the control parameters, especially T_E and N_P, will result in reduced CL values. Moreover, process statistical models were developed using statistical analysis of variance (ANOVA). These models can be used to further understand and control the process within the investigated ranges of control and response parameters.

Keywords: laser drilling; soda-lime glass; nanoliquid; liquid-assisted laser processing; CO_2 laser; ANOVA; Box–Behnken design

Citation: Mahdi, M.N.; Issa, A.; Hasan, H.S.; Al-Hamaoy, A.R.; Hanon, M.M. Influence of Exposure Parameters on Nanoliquid-Assisted Glass Drilling Process Using CO_2 Laser. *Photonics* **2023**, *10*, 89. https://doi.org/10.3390/photonics10010089

Received: 20 October 2022
Revised: 14 December 2022
Accepted: 8 January 2023
Published: 13 January 2023

1. Introduction

Glass and transparent dielectric substances have been commonly used for the production of microfluidic, optical, optoelectronic devices and tools. CO_2 lasers have proven to be effective in processing transparent and dielectric materials with Si-O bonds such as soda-lime glass. This is due to the high absorbance of laser energy by these materials at the emitting wavelengths of CO_2 lasers [1–3]. Previous studies reported that ablation using CO_2 lasers in such materials was obtained using relatively lower power intensities compared to other laser sources [4,5]. The latter makes CO_2 lasers more cost-effective than short-wavelength lasers, plasma etching or wet chemical etching techniques when utilized for micromachining of transparent dielectrics [6,7]. Consequently, and more specifically in the industrial domain, investigative and process statistical modeling studies can be highly beneficial in enhancing process controllability and optimization [8]. Drilling or micro-drilling is one of the fabrication processes aimed to create holes that can serve as couplings, entrance, exit or joining zones in Micro-Electro-Mechanical Systems (MEMS).

Several research works in the literature have been conducted to study the optimal laser drilling process characteristics, control parameters, response parameters and the

produced structures' geometrical identifiers. Uno et al. used a longitudinally excited CO_2 laser to produce crack-free holes in silica glass. The researchers investigated the effects of laser beam power, short laser pulses, pulse energy and gas medium on the drilled hole's characteristics [9]. The drilling of large-aspect-ratio holes in glass is important for the operation of micro-systems. In general, these holes can be used for the inlet/outlet contact of micro-fluidic instruments for biological examination or anodic-bonded silicon-glass. Standard glass drilling by mechanical tools or by laser processing in the air will create many types of defects like bulges, debris cracks and scorch. The liquid-assisted laser processing (LALP) technique has been used to decrease temperature gradient, bulge and heat affected area (HAZ) to produce crack-free glass machined holes [10]. The performance of laser-drilled holes in composite materials is dependent on the thermoset substrate. One of the main factors in laser-drilled polymer composite holes is the heat-affected zone. Consequently, one of the effective ways to minimize the temperature-affected zone is to distribute thermally conductive nanofillers in polymer composites to enhance the heat transfer properties through laser drilling. Some research works showed that by using carbon black, both the heat-affected zone and the taper angle of drilled holes decreased significantly [11]. On the other hand, it is widely accepted that there are various advantages of the LALP drilling process, including minimized/no heat-affected zone, no friction with the machine, high quality, versatility, flexibility, low processing time and low cost [12,13]. Baasandash et al. conducted a study to investigate the laser machinability of three glass types: synthetic quartz, Pyrex glass and soda-lime glass. The researchers investigated the hole production using single-laser-pulse (SLP) drilling and multiple-laser-pulse (MLP) drilling. It was found that the taper angle of a thru-hole can be adjusted with the MLP hole-shaping method, whereby the size coefficient of the pileup around the hole was minimized in synthetic quartz, as compared with SLP drilling [14]. Brusberg et al. used glass as a substrate in interposer applications, which they explain had some advantages compared to traditional packaging materials such as silicon ceramic and polymer founded laminates due to its better insulation and translucent characteristics. The researchers used a CO_2 laser to drill holes that had diameters below 100 µm. They further implemented thermal post-treatment on the substrates to minimize tensile stress and increase reliability. The researchers concluded that it was not possible to obtain a complete crack-free drilling [15]. In another research work, the laser helical drilling technique is applied on aluminum-silicate glass substrates. A femtosecond laser beam with a wavelength of 1552 nm was used to drill holes from the rear side of the substrate to decrease the taper angle. Based on this newly proposed drilling technique, thru-holes were generated with a high roundness quality (<20 µm), a minimal taper angle, low sidewall surface roughness and with small cracks [16]. Synthetic quartz, soda-lime glass and Pyrex glass substrates were drilled using a CO_2 slab waveguide laser centered at a spot size of 130 µm. The researchers used the multiple-pulse hole forming method and it was found to be effective in reducing the height ratio of the pile-up area and the slope angle. Moreover, with single-pulse hole drilling there was a constraint on the exact structure of the hole due to the liquid-phase residual in the hole after the pulse. Furthermore, an optimal number of pulses occurred in the multi-pulse hole cooling and led to precise creation of holes [17]. It was recorded in the literature that mechanical drilling is cost-efficient, simple and potentially suitable for fast manufacturing as it is a mask-less operation. Nevertheless, the thrusting force of the drill acting on the base of the sample easily leads to cracks because of deformation of the glass [18,19]. In general, the glass micro-drilling technology is selected based on the type of the material, and the required hole specifications and equipment properties for a certain device [20–22].

In this paper, it is aimed to study the influence of laser drilling process (control) parameters on the drilled hole's geometrical (response) parameters. The LALP drilling process will be implemented on soda-lime glass sheets immersed in a nanoliquid bath, which is hypothesized to result in improvements on the results obtained from a previous study by the authors using only a water bath [23]. Additionally, initial results of the LALP drilling technique were reported by the authors in a previous study [24]. However, more

focus in this study is given to explaining the effects of all process parameters and relating them to obtained results. Thus far, microscopic inspection of produced holes is performed to measure process response parameters. Furthermore, statistical ANOVA analysis and modeling of results is performed in order to further understand the effects of process control parameters on response parameters.

2. Materials and Methods

The nanoliquid used in this work contained a mixture of carbon nano-particles (CNPs) that had (particle size < 50 nm, assay ≥ 99% trace metals basis and surface area > 100 m^2/g) and de-ionized water. The nanoliquid was used immediately after its preparation so as to avoid any agglomeration problems. Furthermore, the wt.% (0.05, 0.075 and 0.1 wt.%) of CNPs was varied as an experimental control parameter. Figure 1 shows the schematic of the laser drilling setup, which includes a laser source, a reflective mirror, a focal lens and a container to hold immersed glass samples in the nanoliquid bath. The processed samples were sheets of soda-lime glass that had a thickness of 1.1 mm. The samples were affixed 6 mm above the base of the container to avoid inverse reflection of the laser beam, while the samples were also submerged by 1 mm from the top level of the nanoliquid. The nanoliquid was kept at a temperature of 19.7 °C. The laser drilling process was performed using a CA-1500 CW-CO_2 laser work station that has a laser beam source that emits at a wavelength of 10.6 µm and a maximum power of 100 W. The system also included an X-Y sample translation stage carrying the nanoliquid container. The incident CO_2 laser beam was focused to a diameter of 0.25 mm centered on the top surface of the samples using a lens with f = 55 mm.

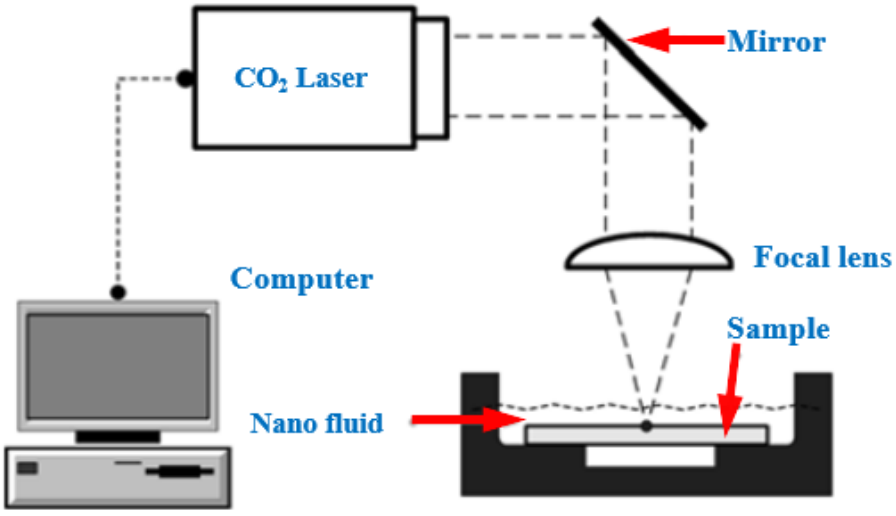

Figure 1. Schematic diagram of the nanoliquid-assisted laser drilling process.

SLP and MLP drilling modes were used to produce holes at various positions on the soda-lime glass sheets. In addition to the wt.% of CNPs, the laser exposure parameters or the experimental control parameters were: laser power (P) varied between 20, 30 and 40 W, exposure time (T_E) of the sample to the incident CW laser beam varied between 0.5, 1 and 1.5 s, and the number of pulses (N_P) delivered to the sample varied between 1, 2, 3, 4, 5 and 6 pulses, these pulses were separated by an idling time of 1 s. The latter parameter does not imply the existence of actual laser pulses, it rather means the number of times the sample is exposed to the CW laser beam. A Genex optical microscope equipped with a digital camera was used to inspect the resulting drilled holes and measure their dimensional features using ImageJ software version 1.52a. The drilled holes' dimensional parameters or experimental response parameters from this work were identified as the crack length (CL, mm) measured at the top surface of the sample, inlet diameter (D_{INLET}, mm) measured at the top surface of the sample and exit diameter (D_{EXIT}, mm) measured at

the bottom surface of the sample. Figure 2 includes microscopic images of some samples showing the measured parameters. It can be seen that CL is measured as the length of the crack extending from the perimeter of D_{INLET} towards the boundaries of the HAZ.

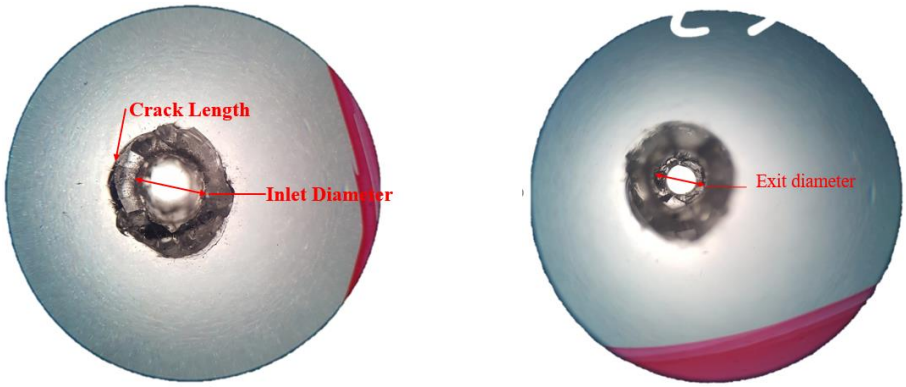

(**a**) (**b**)

Figure 2. Microscopic images of drilled holes and measured parameters: (**a**) CL = 0.287 mm and D_{INLET} = 0.971 mm obtained at 0.075 wt.% CNPs, T_E = 0.5 s, P = 20 W and N_P = 6 pulses, and (**b**) D_{EXIT} = 0.247 mm obtained at 0.1 wt.% CNPs, T_E = 0.5 s, P = 20 W and N_P = 3 pulses.

3. Experimental Results

The dimensional features (CL, D_{INLET} and D_{EXIT}) of the drilled holes are presented in the subsections that follow. This presentation is aimed to show the effect of T_E in combination with different CNPs wt.%, P and N_P values on the resulting dimensional features. It is worth noting that some combinations of process control parameters did not produce measurable hole features; therefore, these data-points were not presented/included in the subsequent figures. However, an explanation of these occurrences is presented in the respective sections that follow.

3.1. Crack Length

This subsection presents the effect of T_E on CL for variable values of P and N_P, and is categorized based on different CNPs wt.% of the nanoliquid bath.

3.1.1. CL Results at 0.1 wt.% CNPs

Figure 3 illustrates CL variation as a result of various T_E and N_P values for each set value of P. The process parameters combination that produces the minimum CL value can be depicted from these results. This minimum CL was recorded at T_E = 0.5 s, N_P = 6 pulses and P = 20 W. In general, it appears that the increase in T_E for all laser beam powers lead to an increase in CL, which can be explained as a direct result of increased impact of induced thermal stresses on the sample surface. Furthermore, increasing N_P is observed to decrease CL for given values of T_E and P, which can be concluded due to the melting of the cracked area with each subsequent laser pulse.

3.1.2. CL Results at 0.075 wt.% CNPs

Figure 4 shows trends and effects similar to those observed for 0.1 wt.% CNPs. It is also apparent that increasing T_E leads to increasing the value of CL for all set values of laser beam power. Furthermore, increasing N_P for fixed T_E and P values causes a decrease in CL values due to further melting of the cracked zone with subsequent laser pulses. The minimum CL value was recorded for T_E = 0.5 s, N_P = 6 pulses and P = 20 W.

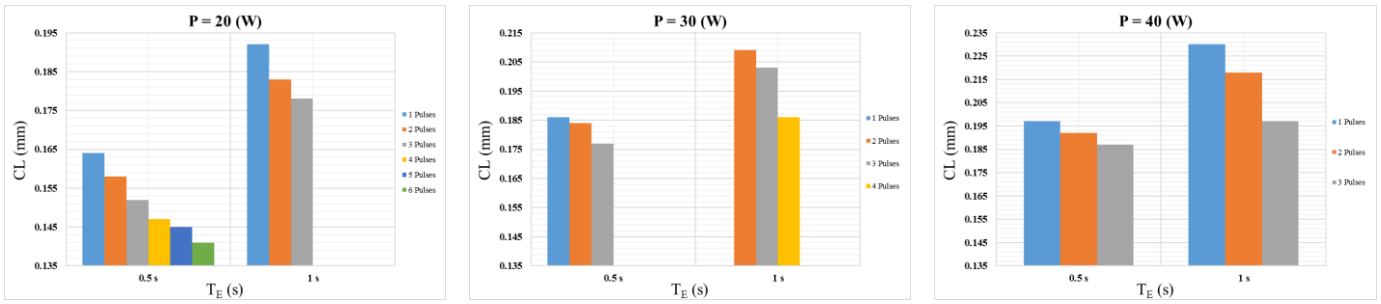

(**a**) (**b**) (**c**)

Figure 3. Influence of T_E and N_P on CL for 0.1 wt.% of CNPs and (**a**) P = 20 W, (**b**) P = 30 W and (**c**) P = 40 W.

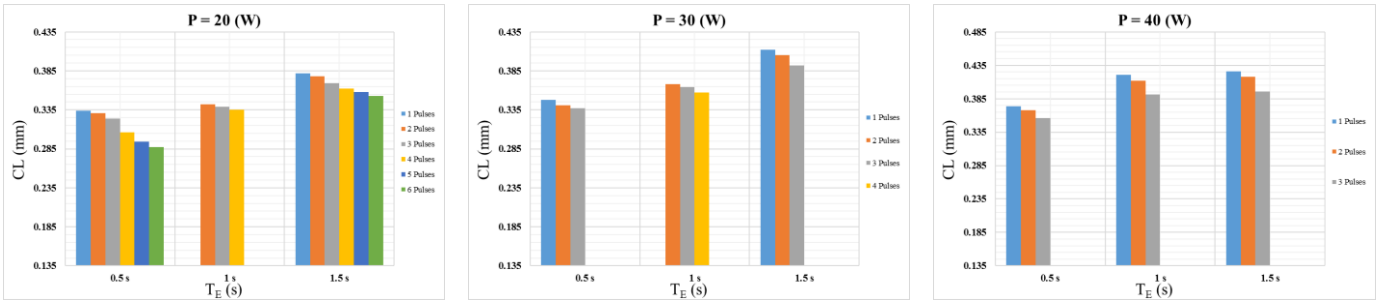

(**a**) (**b**) (**c**)

Figure 4. Influence of T_E and N_P on CL for 0.075 wt.% of CNPs and (**a**) P = 20 W, (**b**) P = 30 W and (**c**) P = 40 W.

3.1.3. CL Results at 0.05 wt.% CNPs

Figure 5 shows trends and effects similar to those observed for 0.1 wt.% and 0.075 wt.% CNPs. It can be seen that increasing T_E leads to increasing the value of CL for all set values of laser beam power. Furthermore, increasing N_P for given T_E and P values decreases CL due to further melting of the cracked zone with subsequent laser pulses. The minimum CL value was recorded for T_E = 0.5 s, N_P = 6 pulses and P = 20 W.

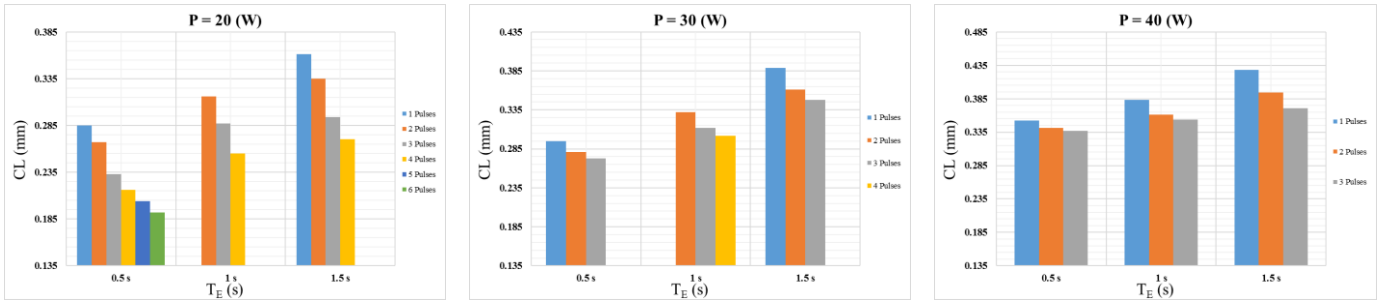

(**a**) (**b**) (**c**)

Figure 5. Influence of T_E and N_P on CL for 0.05 wt.% of CNPs and (**a**) P = 20 W, (**b**) P = 30 W and (**c**) P = 40 W.

3.2. Inlet Diameter

This subsection presents the effect of T_E on D_{INLET} for variable values of P and N_P, and is categorized based on different CNPs wt.% of the nanoliquid bath.

3.2.1. D_{INLET} Results at 0.1 wt.% CNPs

Figure 6 shows the variations in D_{INLET} for different values of T_E and N_P and is grouped for each set value of P. The processing parameters combined to produce the minimum D_{INLET} can be observed at T_E = 0.5 s, N_P = 1 pulse and P = 20 W. It is easy to depict that increasing T_E causes increased D_{INLET} for a given value of P, which can be explained as a result of more energy deposited in the glass sample and, consequently, larger HAZ and ablated mass. Furthermore, it is natural to conclude that increasing N_P for a given T_E and P value will also lead to increasing D_{INLET}.

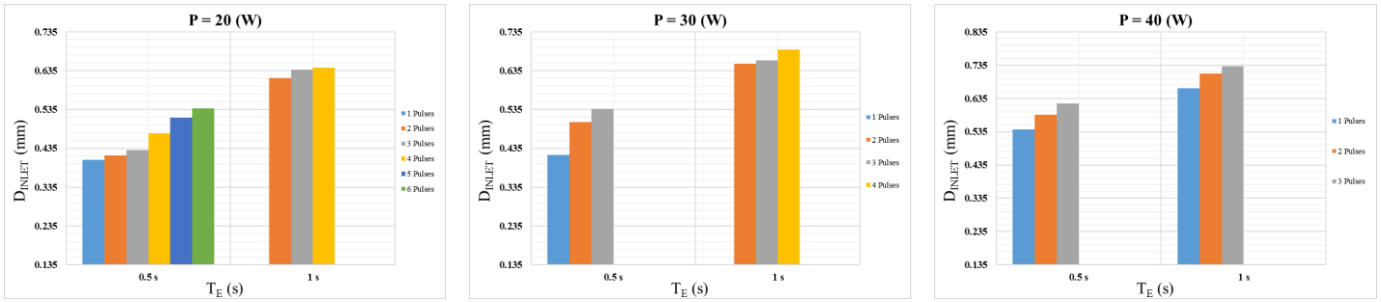

(**a**) (**b**) (**c**)

Figure 6. Influence of T_E and N_P on D_{INLET} for 0.1 wt.% of CNPs and (**a**) P = 20 W, (**b**) P = 30 W and (**c**) P = 40 W.

3.2.2. D_{INLET} Results at 0.075 wt.% CNPs

Figure 7 illustrate values and behaviors similar to those observed for 0.1 wt.% CNPs. It is also evident that increasing T_E leads to increasing the value of D_{INLET} for all set values of laser beam power. Furthermore, increasing N_P for fixed T_E and P values causes an increase in D_{INLET} values due to further ablation with subsequent laser pulses. The minimum D_{INLET} value was recorded for T_E = 0.5 s, N_P = 1 pulse and P = 20 W.

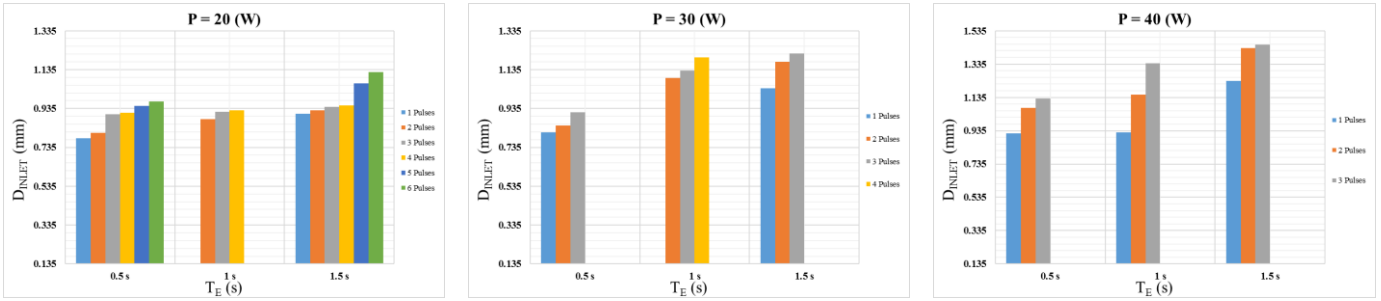

(**a**) (**b**) (**c**)

Figure 7. Influence of T_E and N_P on D_{INLET} for 0.075 wt.% of CNPs and (**a**) P = 20 W, (**b**) P = 30 W and (**c**) P = 40 W.

3.2.3. D_{INLET} Results at 0.05 wt.% CNPs

Figure 8 shows trends and effects similar to those observed for 0.1 wt.% and 0.075 wt.% CNPs. It can be seen that increasing T_E leads to increasing the value of D_{INLET} for all set values of laser beam power. Furthermore, increasing N_P for given T_E and P values increases D_{INLET} due to further ablation of material with subsequent laser pulses. The minimum D_{INLET} value was recorded for T_E = 0.5 s, N_P = 1 pulse and P = 20 W.

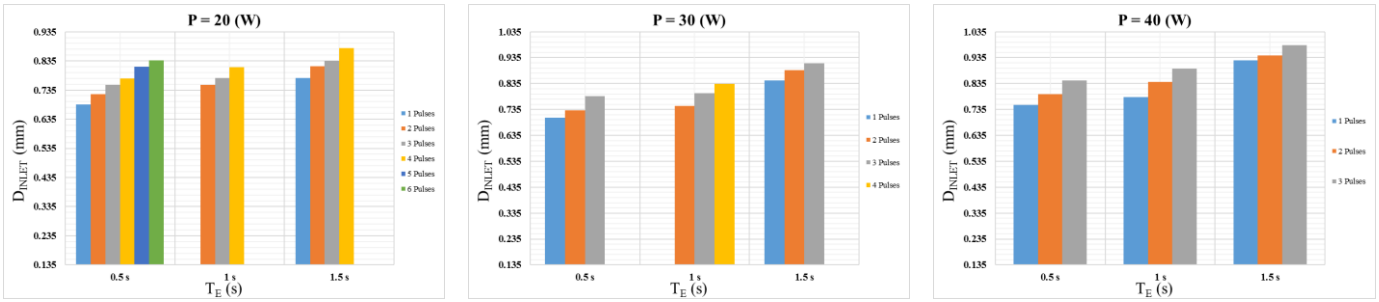

(**a**) (**b**) (**c**)

Figure 8. Influence of T_E and N_P on D_{INLET} for 0.05 wt.% of CNPs and (**a**) P = 20 W, (**b**) P = 30 W and (**c**) P = 40 W.

It is worth mentioning that in the preceding two sections some CL and D_{INLET} values were not measurable and could not be presented. These incidences were either due to insufficient laser power to initiate ablation (e.g., low T_E combined with low P and/or low N_P) or due to excessive incident laser power that caused sample damage (e.g., high T_E combined with high P and/or high N_P).

3.3. Exit Diameter

This subsection presents the effect of T_E on D_{EXIT} for variable values of P and N_P, and is categorized based on different CNPs wt.% of the nanoliquid bath.

3.3.1. D_{EXIT} Results at 0.1 wt.% CNPs

Figure 9 shows the effects of T_E and N_P on D_{EXIT} grouped for each set value of P. The combinations of processing parameters that result in the minimum D_{EXIT} can be observed at T_E = 0.5 s, N_P = 3 pulses and P = 20 W. It is obvious that increasing T_E causes increased D_{EXIT} for a given value of P, which can be explained as a result of more energy deposited in the glass sample and, consequently, larger HAZ and ablated mass. Furthermore, it is natural to conclude that increasing N_P for a given T_E and P value will also lead to increasing D_{EXIT}.

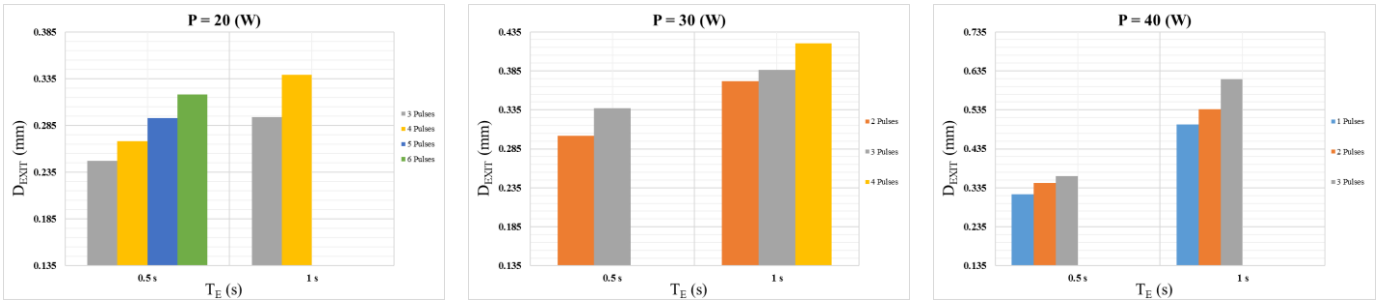

(**a**) (**b**) (**c**)

Figure 9. Influence of T_E and N_P on D_{EXIT} for 0.1 wt.% of CNPs and (**a**) P = 20 W, (**b**) P = 30 W and (**c**) P = 40 W.

3.3.2. D_{EXIT} Results at 0.075 wt.% CNPs

Figure 10 illustrates values and behaviors similar to those observed for 0.1 wt.% CNPs. It is also evident that increasing T_E leads to increasing the value of D_{EXIT} for all set values of laser beam power. Furthermore, increasing N_P for fixed T_E and P values causes an increase in D_{EXIT} values due to further ablation with subsequent laser pulses. The minimum D_{EXIT} value was recorded for T_E = 0.5 s, N_P = 6 pulses and P = 20 W.

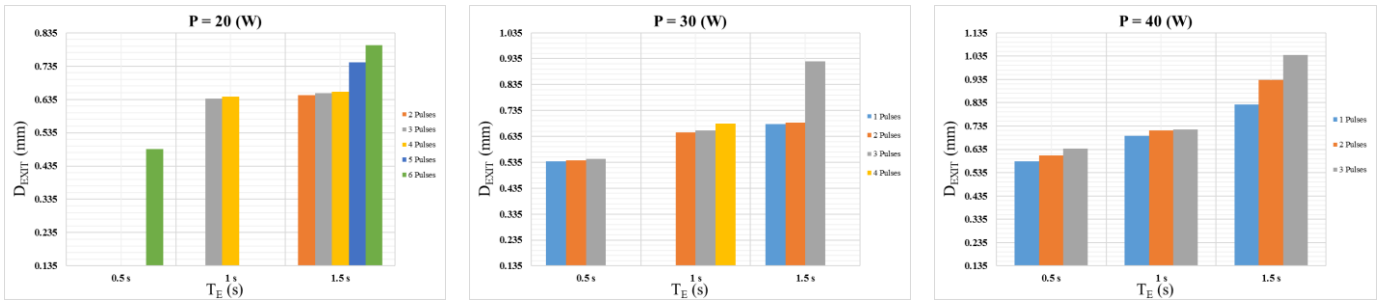

(**a**) (**b**) (**c**)

Figure 10. Influence of T_E and N_P on D_{EXIT} for 0.1 wt.% of CNPs and (**a**) P = 20 W, (**b**) P = 30 W and (**c**) P = 40 W.

3.3.3. D_{EXIT} Results at 0.05 wt.% CNPs

Figure 11 shows trends and effects similar to those observed for 0.1 wt.% and 0.075 wt.% CNPs. It can be seen that increasing T_E leads to increasing the value of D_{EXIT} for all set values of laser beam power. Furthermore, increasing N_P for given T_E and P values increases D_{EXIT} due to further ablation of the material with subsequent laser pulses. The minimum D_{EXIT} value was recorded for T_E = 0.5 s, N_P = 5 pulses and P = 20 W.

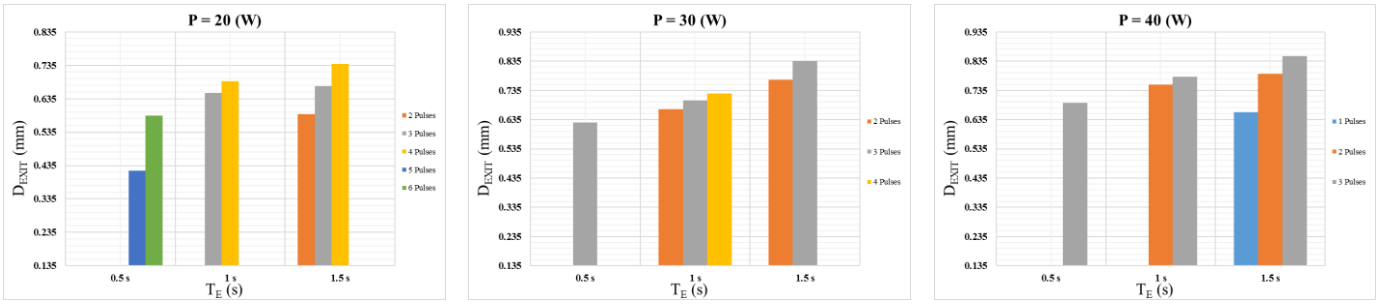

(**a**) (**b**) (**c**)

Figure 11. Influence of T_E and N_P on D_{EXIT} for 0.05 wt.% of CNPs and (**a**) P = 20 W, (**b**) P = 30 W and (**c**) P = 40 W.

It is worthy to note from the results presented in this section that some samples did not exhibit a measurable D_{EXIT}. This observation implies that low values of power, T_E or N_P were delivered, either individually or in combination, which was not sufficient to create a thru-hole.

4. ANOVA Modeling

The statistical analysis of variance (ANOVA) is presented in this section for the obtained dataset/results from the experiments conducted in this work. To perform ANOVA, the process control parameters were chosen to be T_E, P and N_P. Furthermore, each wt.% of CNPs was treated as a separate block of experiments. Therefore, three sets of experimental designs were built in order to derive a regression model of the drilling process. These models can be used to relate the process control parameters to the process response parameters, CL and D_{INLET}. Moreover, the models can be used to predict the response value for a certain combination of control parameter values that were not actually tested. To achieve the aforementioned models, a Box–Behnken experimental design was implemented using the StatEase DesignExpert software v.11. This software has capabilities of building regression models using Response Surface Methodology (RSM). The following subsections present the obtained ANOVA mathematical model and 3D response surfaces relating control parameters to response parameters for each wt.% of CNPs. Each 3D response surface in the subsequent sections indicates the effects of T_E and P as control parameters at a certain

value of N_P. Moreover, each mathematical model can be used to predict the values of CL and D_{INLET} using different combinations of T_E, P and N_P values. Furthermore, plots of normal residuals for each model are presented to show the model fitness and adequacy in representing the experimental data.

4.1. ANOVA for 0.1 wt.% CNPs

4.1.1. Crack Length

Figure 12a shows the 3D response surface relating CL to T_E and P for N_P = 2.48. Figure 12b displays the normal residuals for the CL model. The mathematical model found as a result of ANOVA in terms of the actual control parameters is given by

$$\boldsymbol{CL} = 0.195 + 0.0152 \times T_E + 0.015 \times P - 7.80 \times 10^{-3} \times N_P - 2.1954 \times 10^{-3} \times T_E \times P + 2.876 \times 10^{-3} \times T_E \times N_P + 4.848 \times 10^{-4} \times P \times N_P + 0.0 \times T_E^2 + 5.797 \times 10^{-3} \times P^2 + 1.411 \times 10^{-3} \times N_P^2 \quad (1)$$

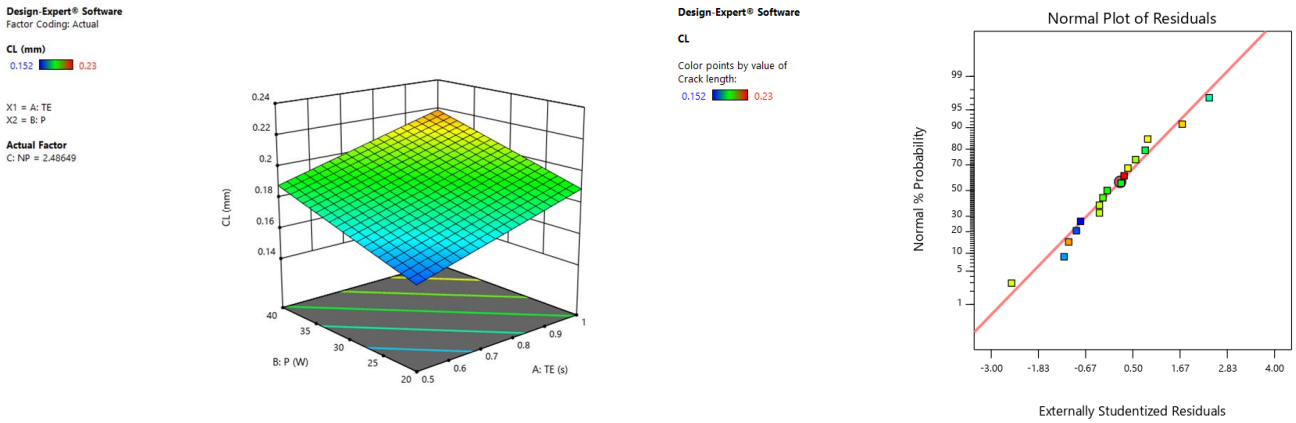

(**a**) (**b**)

Figure 12. ANOVA model results for CL at 0.1 wt.% CNPs: (**a**) 3D response surface and (**b**) normal residuals plot.

4.1.2. Inlet Diameter

Figure 13a shows the 3D response surface relating D_{INLET} to T_E and P for N_P = 1.51. Figure 13b displays the normal residuals for the D_{INLET} model. The mathematical model found as a result of ANOVA in terms of the actual control parameters is given by

$$\boldsymbol{D_{INLET}} = 0.564 + 0.079 \times T_E + 0.064 \times P + 0.028 \times N_P - 0.023 \times T_E \times P - 0.0148 \times T_E \times N_P + 0.022 \times P \times N_P + 0.0 \times T_E^2 + 0.019 \times P^2 - 6.85 \times 10^{-4} \times N_P^2 \quad (2)$$

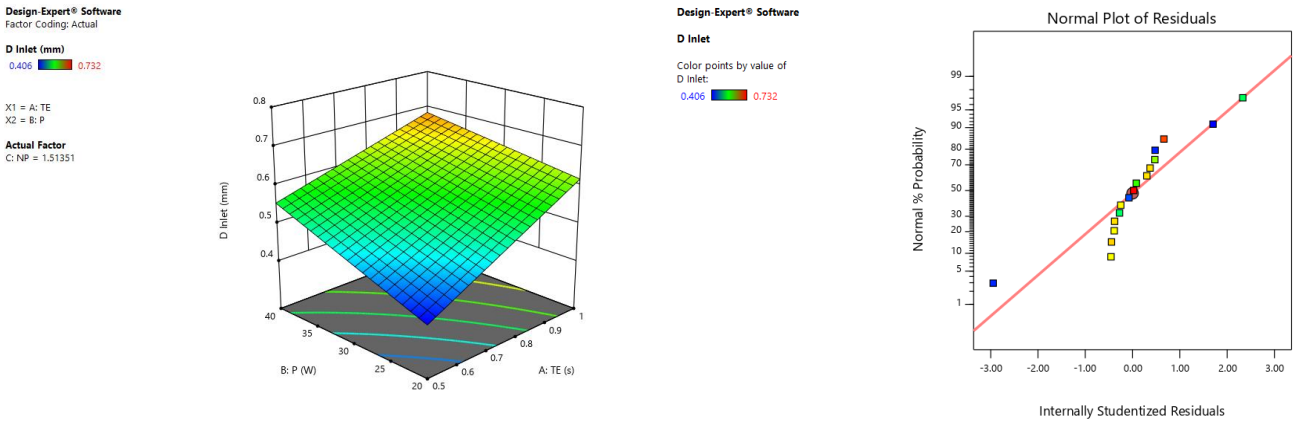

(**a**) (**b**)

Figure 13. ANOVA model results for D_{INLET} at 0.1 wt.% CNPs: (**a**) 3D response surface and (**b**) normal residuals plot.

4.2. ANOVA for 0.075 wt.% CNPs

4.2.1. Crack Length

Figure 14a shows the 3D response surface relating CL to T_E and P for N_P = 2.37. Figure 14b displays the normal residuals for the CL model. The mathematical model found as a result of ANOVA in terms of the actual control parameters is given by

$$\boldsymbol{CL} = 0.36897 + 0.027 \times T_E + 0.0241152 \times P - 0.016524 \times N_P + 7.50001 \times 10^{-4} \times T_E \times P - 2.250 \times 10^{-3} \times T_E \times N_P - 1.6121724 \times 10^{-3} \times P \times N_P + 1.50517 \times 10^{-3} \times T_E^2 + 6.20 \times 10^{-3} \times P^2 + 6.143 \times 10^{-3} \times N_P^2 \quad (3)$$

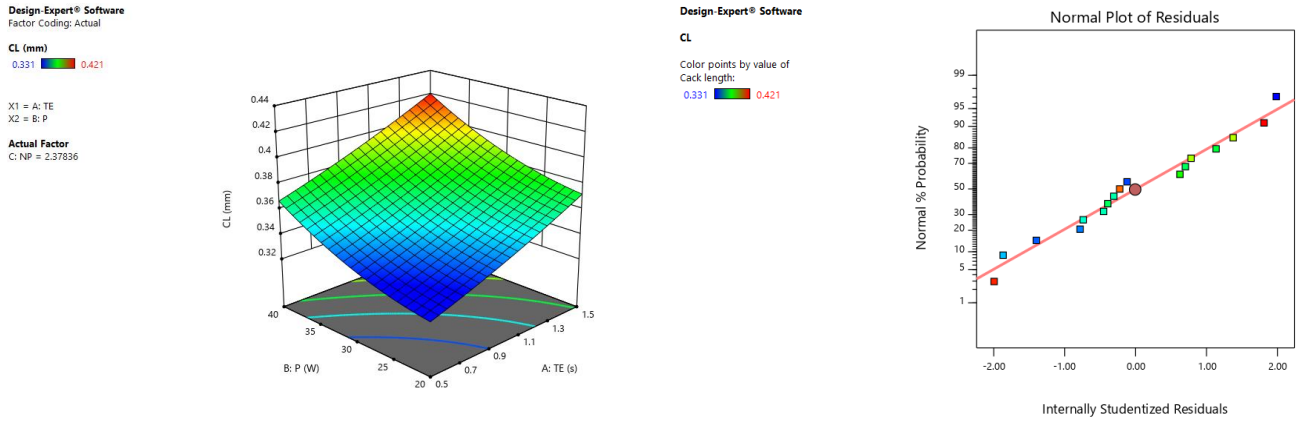

(**a**) (**b**)

Figure 14. ANOVA model results for CL at 0.075 wt.% CNPs: (**a**) 3D response surface and (**b**) normal residuals plot.

4.2.2. Inlet Diameter

Figure 15a shows the 3D response surface relating D_{INLET} to T_E and P for N_P = 1.94. Figure 15b displays the normal residuals for the D_{INLET} model. The mathematical model found as a result of ANOVA in terms of the actual control parameters is given by

$$\boldsymbol{D_{INLET}} = 0.973 - 0.207 \times T_E - 0.014 \times P - 0.075 \times N_P + 0.012 \times T_E \times P + 1.664 \times 10^{-3} \times T_E \times N_P + 5.172 \times 10^{-3} \times P \times N_P + 0.0306 \times T_E^2 + 1.1469 \times 10^{-4} \times P^2 + 1.409 \times 10^{-3} \times N_P^2 \quad (4)$$

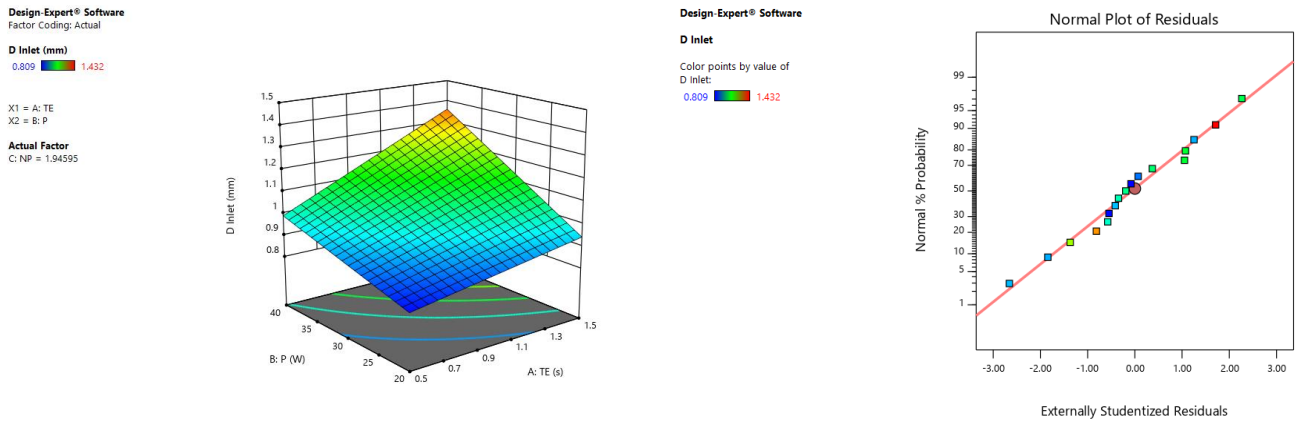

(**a**) (**b**)

Figure 15. ANOVA model results for D_{INLET} at 0.075 wt.% CNPs: (**a**) 3D response surface and (**b**) normal residuals plot.

4.3. ANOVA for 0.05 wt.% CNPs

4.3.1. Crack Length

Figure 16a shows the 3D response surface relating CL to T_E and P for N_P = 2.48. Figure 16b displays the normal residuals for the CL model. The mathematical model found as a result of ANOVA in terms of the actual control parameters is given by

$$\boldsymbol{CL} = 0.335 + 0.0362 \times T_E + 0.0314 \times P - 0.016 \times N_P - 3.750 \times 10^{-3} \times T_E \times P - 4.750 \times 10^{-3} \times T_E \times N_P + 2.284 \times 10^{-3} \times P \times N_P - 6.310 \times 10^{-3} \times T_E^2 + 6.258 \times 10^{-3} \times P^2 - 3.275 \times 10^{-3} \times N_P^2 \quad (5)$$

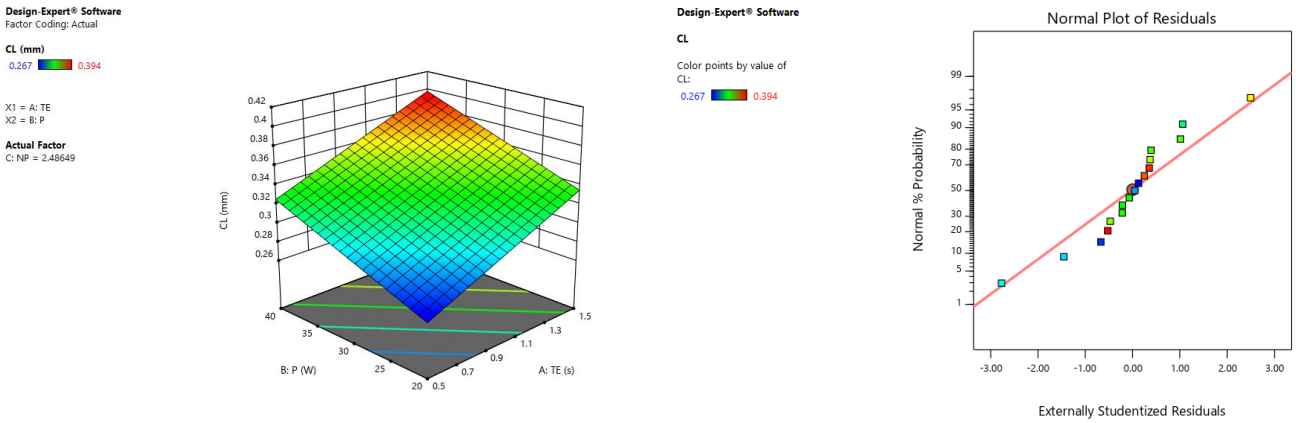

(**a**) (**b**)

Figure 16. ANOVA model results for CL at 0.05 wt.% CNPs: (**a**) 3D response surface and (**b**) normal residuals plot.

4.3.2. Inlet Diameter

Figure 17a shows the 3D response surface relating D_{INLET} to T_E and P for N_P = 1.64. Figure 17b displays the normal residuals for the D_{INLET} model. The mathematical model found as a result of ANOVA in terms of the actual control parameters is given by

$$\boldsymbol{D_{INLET}} = 0.755 + 0.0643 \times T_E + 0.043 \times P + 0.0381 \times N_P + 0.0132 \times T_E \times P - 4.0 \times 10^{-3} \times T_E \times N_P + 0.01618 \times P \times N_P + 0.039 \times T_E^2 + 0.0260 \times P^2 + 0.0159 \times N_P^2 \quad (6)$$

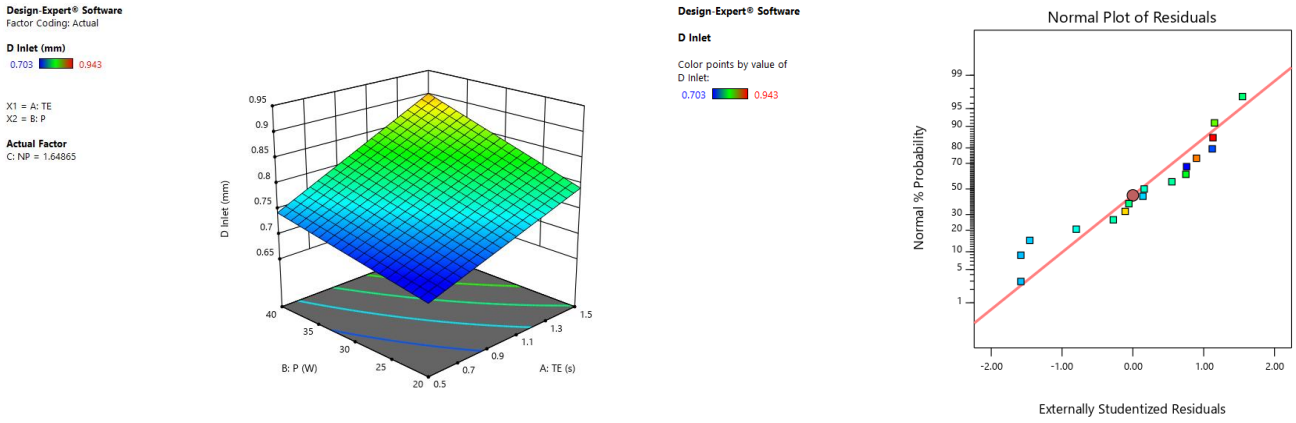

(**a**) (**b**)

Figure 17. ANOVA model results for D_{INLET} at 0.05 wt.% CNPs: (**a**) 3D response surface and (**b**) normal residuals plot.

Following the statistical analysis of results and models, it can be seen that there is an agreement in the effects of T_E, P and N_P on resulting CL and D_{INLET} presented in the previous section. Looking at the ANOVA model Equations (1) to (6), the numeric

coefficient values of the control parameters T_E, P and N_P, in their pure forms, depict they have the most significant impacts on the response parameters CL and D_{INLET}. The model equations also include less significant terms such as $T_E \times P$ and $(N_P)^2$, which account for the interactive/combined effects of the control parameters on the response parameters. The model equations and 3D response surfaces for CL and D_{INLET} were validated by using them to predict certain response values, then conducting the experiment and measuring the actual response value. The validation experiment results shown in Table 1 were conducted for combinations of process control parameters that were not used in the derivation of the models. It can be seen from the results in Table 1 that the models are very accurate in fitting the experimental data and consequently in predicting response parameters within the investigated range of control parameters.

Table 1. ANOVA models validation: predicted and experimental response values for different combinations of process control parameters.

	wt.%	T_E (s)	P (W)	N_P (Pulses)	CL (mm) Predicted	CL (mm) Experimental
Sample 1	0.1	0.5	20	6	0.1538	0.141
Sample 2	0.1	1	40	2	0.217	0.218
Sample 3	0.075	1.5	20	5	0.356	0.358
Sample 4	0.075	0.5	40	2	0.361	0.368
	wt.%	T_E (s)	P (W)	N_P (Pulses)	D_{INLET} (mm) Predicted	D_{INLET} (mm) Experimental
Sample 5	0.1	0.5	20	4	0.476	0.473
Sample 6	0.1	1	40	3	0.735	0.732
Sample 7	0.075	0.5	20	6	0.983	0.971
Sample 8	0.075	1.5	40	2	1.396	1.432

5. Overall Discussion of Findings

Based on results presented in previous sections, it can be seen that increasing T_E for given values of P or N_P tends to increase the values of CL, D_{INLET} and D_{EXIT}. This is directly understood to be the effect of more time allowed for thermal stresses to create crack zones as well as more time allowed for depositing more laser power to increase HAZ and, consequently, ablation zones. Furthermore, close examination of the results reveals that increasing P or N_P also led to increasing the response parameters CL, D_{INLET} and D_{EXIT} for given T_E or wt.% values. Moreover, the change in wt.% of CNPs does not seem to have a great impact on the resulting CL, D_{INLET} or D_{EXIT} as compared to the influence of the other control parameters T_E, P and N_P. However, there is a general increase in the values of CL, D_{INLET} and D_{EXIT} as wt.% is altered from 0.1% to 0.075%, followed by a decrease in these response values as wt.% is further reduced from 0.075% to 0.05%. This can be observed by looking across all blocks of the experimental results. Nevertheless, and more importantly, it is worth noting that the nanoliquid bath with CNPs was very essential for producing acceptable and finely drilled holes as compared with initial results obtained from drilling holes in dry air conditions, which mostly resulted in fractured samples as shown in Figure 18.

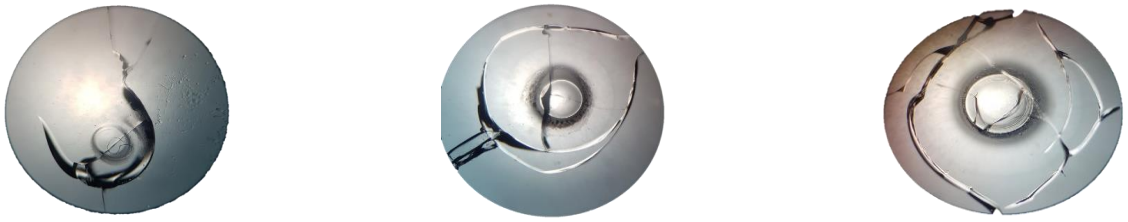

(**a**) (**b**) (**c**)

Figure 18. Holes drilled in air: (**a**) T_E = 1 s, P = 5 W, N_P = 2 pulse, (**b**) T_E = 2 s, P = 10 W, N_P = 1 pulses and (**c**) T_E = 2 s, P = 15 W, N_P = 1 pulse.

As compared to observations in a previous study performed by the authors [23], the use of a nanoliquid bath and the incorporation of CNPs resulted in decreased levels of T_E needed to perform underwater drilling of holes. T_E values ranged from 5 s to 10 s in [23], as compared to 0.5 s to 1.5 s in this study. This means that there is a significant decrease in power consumption and a reduction of cost as a direct effect. Furthermore, from quality and accuracy perspectives, CL values can be seen to have reduced, in general, comparing the two studies. The latter can be explained as a direct benefit of CNPs in decreasing the temperature gradients surrounding the drilled holes by effectively cooling the molten surface and, consequently, decreasing the HAZ. Therefore, the utilization of a nanoliquid bath with CNPs can be concluded to have enhanced the surface performance by decreasing the induced micro-crack lengths. The latter can be physically explained by envisioning CNPs to act as a factor limiting the thermal damage around the drilled holes by enhancing the effective thermal conductivity of the medium.

6. Conclusions

Following the discussion of the results and findings of this research work, it can be concluded that the nanoliquid bath and MLP drilling paradigm implemented reduces the crack lengths (CL) in the processed samples due to effective heat dissipation into the nanoliquid bath and further melting and vaporization of the cracked zone with successive laser pulses. Furthermore, increasing the exposure time (T_E) alone leads to increasing the crack length (CL) as well as increasing the hole inlet and exit diameters (D_{INLET} and D_{EXIT}). Keeping in mind that CL is not a desirable feature to increase, maintaining a good balance among the control parameters, especially T_E and $N_{P,}$ will result in reduced CL values.

The experimental results and investigated range of control parameter combinations produced promising results with CL range (0.141 to 0.428 mm), D_{INLET} range (0.406 to 1.452 mm) and D_{EXIT} range (0.247 to 1.039 mm). These results can be further tested and verified to develop reliable and repeatable laser drilling guidelines in soda-lime glass using the nanoliquid bath technique and the CO_2 laser setup at hand. The latter can be very beneficial in conducting studies to investigate other response parameters such as hole taper angle, roundness and surface roughness. This will allow for drilling holes with controlled feathers and specifications to suit certain applications such as microfluidic devices and microdevices for light coupling or transmission. Future studies will include thermal simulation of the process to further understand the physical interactions of the material, laser irradiation and the nanoliquid bath leading to deeper explanation of the results.

Finally, the statistical models developed using ANOVA analysis for the investigated ranges of control and response parameters can be used to further understand, optimize and control the process, especially when there is a demand to scale up the results to suit industrial implementation. The derived models are capable of introducing the possibility to predict certain response values or derive certain control parameter values based on desirable process outcomes.

Author Contributions: Conceptualization, A.R.A.-H. and H.S.H.; methodology, A.R.A.-H., H.S.H. and M.N.M.; software, M.N.M.; validation, H.S.H., M.N.M. and A.I.; formal analysis, A.R.A.-H.; investigation, M.N.M.; resources, M.M.H.; data curation, M.N.M.; writing—original draft preparation, M.N.M.; writing—review and editing, A.R.A.-H., H.S.H., A.I. and M.M.H.; visualization, A.R.A.-H.; supervision, A.R.A.-H. and H.S.H.; project administration, A.R.A.-H.; funding acquisition, M.M.H. All authors have read and agreed to the published version of the manuscript.

Funding: This research received no external funding.

Institutional Review Board Statement: Not applicable.

Informed Consent Statement: Not applicable.

Data Availability Statement: The data used to support this study's findings can be provided by the corresponding author upon reasonable request.

Conflicts of Interest: The authors declare no conflict of interest.

References

1. Buerhop, C.; Blumenthal, B.; Weissmann, R.; Lutz, N.; Biermann, B. Glass surface treatment with excimer and CO_2 lasers. *Appl. Surf. Sci.* **1990**, *46*, 430–434. [CrossRef]
2. Kozhukharov, V.; Dimitrov, D.; Tonchev, D. Integration of CO_2 laser radiation with glasses. *Infrared Phys.* **1989**, *29*, 415–422. [CrossRef]
3. Isard, J.O. Surface reflectivity of strongly absorbing media and calculations of the infrared emissivity of glass. *Infrared Phys.* **1979**, *20*, 249–256. [CrossRef]
4. Miller, J.C. *Laser Ablation: Principles and Applications*; Springer-Verlag: Berlin, Germany, 1994.
5. Lee, Y.-I.; Song, K.; Sneddon, J. *Laser-Induced Breakdown Spectrometry*; Nova Science Publishers, Inc.: Huntington, NY, USA, 2000.
6. Wang, S.-C.; Lee, C.-Y.; Chen, H.-P. Thermoplastic microchannel fabrication using carbon dioxide laser ablation. *J. Chromatogr. A* **2006**, *1111*, 252–257. [CrossRef] [PubMed]
7. Chung, C.K.; Wu, M.; Wu, J.; Sung, Y.; Huang, G.R. Silicon micromachining by CO_2 laser. In Proceedings of the 1st IEEE International Conference on Nano/Micro Engineered and Molecular Systems, Zhuhai, China, 18–21 January 2006; pp. 1445–1448.
8. Issa, A. Computational Control of Laser Systems For Micro-Machining. Ph.D. Thesis, Dublin City University, Dublin, Ireland, 2007.
9. Uno, K.; Yamamoto, T.; Akitsu, T.; Jitsuno, T. Glass drilling by longitudinally excited CO_2 laser with short laser pulse. In Proceedings of the Laser Applications in Microelectronic and Optoelectronic Manufacturing (LAMOM) XX, San Francisco, CA, USA, 7–12 February 2015. [CrossRef]
10. Chung, C.K.; Lin, S.L. CO2 laser micromachined crackless through holes of Pyrex 7740 glass. *Int. J. Mach. Tools Manuf.* **2010**, *50*, 961–968. [CrossRef]
11. Nagesh, S.; Murthy, H.N.; Krishna, M.; Basavaraj, H. Parametric study of CO_2 laser drilling of carbon nanopowder/vinylester/glass nanocomposites using design of experiments and grey relational analysis. *Opt. Laser Technol.* **2013**, *48*, 480–488. [CrossRef]
12. Kannatey-Asibu, E. *Principles of Laser Materials Processing*; John Wiley & Sons, Inc.: Hoboken, NJ, USA, 2009.
13. Maini, A.K. *Lasers and Optoelectronics: Fundamentals, Devices and Applications*; John Wiley and Sons Ltd.: West Sussex, UK, 2013.
14. Baasandash, C.; Yabe, T.; Maehara, J.; Yamaguchi, M.; Wakatsuki, H. Crack-Free High-Aspect-Ratio Drilling of Glasses by 1 μm Yttrium Aluminum Garnet Laser and Translucent Adhesive Tape. *Jpn. J. Appl. Phys. Part 2 Lett.* **2004**, *43*, L133–L135. [CrossRef]
15. Brusberg, L.; Queisser, M.; Neitz, M.; Schroder, H.; Lang, K.D. CO2-Laser drilling of TGVs for glass interposer applications lars. In Proceedings of the 2014 IEEE 64th Electronic Components and Technology Conference (ECTC), Orlando, FL, USA, 27–30 May 2014. [CrossRef]
16. Lee, H.M.; Choi, J.; Moon, S.J. Determining the machining parameters for femtosecond laser helical drilling of aluminosilicate glass substrate. *Int. J. Precis. Eng. Manuf.* **2017**, *18*, 923–930. [CrossRef]
17. Ogur, H.; Yoshida, Y. Hole Drilling of Glass Substrates with a Slab Waveguide CO2 Laser. *Jpn. J. Appl. Phys. Part 1 Regul. Pap. Short Notes Rev. Pap.* **2000**, *42*, 2881–2886. [CrossRef]
18. Yoon, H.-S.; Chung, S.-C. *Inspection of Micro-Drilling Processes by Using the On-Machine Vision, Focus (Madison)*; 2005.
19. Park, B.J.; Choi, Y.; Chu, C.N. Prevention of exit crack in mirco drilling of soda-lime glass. *CIRP Ann. Manuf. Technol.* **2002**, *51*, 347–350. [CrossRef]
20. Noori, A.; Upadhyaya, S.; Selvanganapathy, P.R. Materials and microfabrication processes for microfluidic devices. In *Microfluidics for Biological Applications*; Tian, W.C., Finehout, E., Eds.; Springer: Boston, MA, USA, 2008; pp. 35–92. [CrossRef]
21. Iliescu, C.; Tay, F.; Miao, J. Strategies in deep wet etching of Pyrex glass. *Sens. Actuators A Phys.* **2007**, *133*, 395–400. [CrossRef]
22. Iliescu, C.; Taylor, H.; Avram, M.; Miao, J.; Franssila, S. A practical guide for the fabrication of microfluidic devices using glass and silicon. *Biomicrofluidics* **2012**, *6*, 016505. [CrossRef] [PubMed]
23. Auda, L.H.; Al-Hamaoy, A.R. Effect of power on hole quality of underwater glass drilling using CO_2 laser. *J. Eng. Sustain. Dev.* **2020**, *24*, 59–65. [CrossRef]
24. Mahdi, M.N.; Al-Hamaoy, A.R.; Hasan, H.S. Effect of nano fluid and number of pulses on glass drilling using CO_2 laser. *AIP Conf. Proc.* **2021**, *2372*, 080025. [CrossRef]